Contents lists available at ScienceDirect

Arabian Journal of Chemistry

journal homepage: www.ksu.edu.sa

Original article

U(VI) sorption by porous sodium zirconium phosphate pellets from aqueous solution

Cheng Wang [a], Bingtao Gui [a], Tianjie Li [a], Ruiyang Chang [a], Junxiang Shu [a], Xiaoqin Deng [c], Li Chen [c], Maodan Luo [c], Bing Jiang [c], Su Xu [c], Juan Zhai [a,d], Jun Liu [a,d,**], Changsong Zhao [b,*]

[a] College of Nuclear Technology and Automation Engineering, Chengdu University of Technology, Chengdu 610059, Sichuan, PR China
[b] School of Public Health, Chengdu Medical College, Chengdu 610500, Sichuan, PR China
[c] Sichuan Management and Monitoring Center Station of Radioactive Environment, Chengdu 610059, Sichuan, PR China
[d] Applied Nuclear Technology in Geosciences Key Laboratory of Sichuan Province, Chengdu University of Technology, Chengdu 610059, Sichuan, PR China

ARTICLE INFO

Keywords:
Porous sodium zirconium phosphate pellets
Static/dynamic sorption
U(VI)
Mechanism
Rare earth wastewater

ABSTRACT

Zirconium phosphate is the first artificially produced layered phosphate that can sorb a variety of nuclides from solutions. Sodium zirconium phosphate (NZP) was a type of α-zirconium phosphate (α-ZrP). The porous sodium zirconium phosphate pellets (p-NZP-P) with a diameter of more than ~3 mm were prepared and used for uranium sorption. The p-NZP-P could be immersed in solutions for more than 5 days without dissolving and structurally collapsing. The sorption properties of U(VI) on p-NZP-P in solutions were investigated by both static and dynamic sorption tests. Synthetic p-NZP-P was analyzed in detail using various characterizations to investigate their character and structural changes. In the static sorption experiment, the equilibrium sorption capacity reached the 77.5 ± 1.5 mg·g^{-1} when the initial concentration of U(VI) was 100 mg/L, $pH_{initial}$ = 4.5, T = 25 ℃. Uranium sorption increased by ~69 % and ~215 %, respectively, when the initial uranium concentration was increased from 100 to 300 mg·L^{-1} and the temperature was increased from 15 to 55 °C. Furthermore, uranium sorption increased by ~541 % when the initial pH increased from 2.5 to 4.5, while it decreased by ~39 % when the initial pH increased from 4.5 to 7.0. The sorption data corresponded to the pseudo-second-order kinetic model and the Langmuir isotherm model, as well as the theoretically predicted value of sorption capacity (~199.9 mg·g^{-1}). The results of the dynamic sorption experiment showed that decreasing the quality, increasing the flow rate and the initial U(VI) concentration would shorten the breakthrough time. The dynamic sorption data agreed well with the Thomas model. The characterization confirmed the porous properties, while the U(VI) sorption mechanisms relate to –OH coordination and ion exchange. A radioactive rare earth wastewater treatment test suggested that p-NZP-P could be the potential uranium sorbent due to its good stability and efficiency. This paper opened opportunities for the development of practical materials for treating radioactive wastewater in the application of actual scenarios.

1. Introduction

With the continuous development of the economy, due to the increasing demand for energy, there was an urgent need to adapt and diversify the energy structures. Among new energy candidates, nuclear energy had obvious economic and environmental advantages. Uranium is an important mineral resource in the nuclear industry, its scarcity increases the value of fuel recycling (Pei et al., 2024; Rajesh and Dhanaraj, 2023; Yusop et al., 2023). However, as the main pollutant nuclide in radioactive wastewater, uranium has a significantly longer half-life and stronger muscle toxicity compared to other pollutants and can easily migrate in the natural environment (Attallah et al., 2024; Attallah et al., 2017; Ma et al., 2023). In addition, radioactive wastewater from nuclear power plants, factories, agricultural production scientific research organizations or unconventional uranium resource has a wider range of uranium concentrations, and the species of uranium are more complex (Haneklaus, 2021). Therefore, the efficient and economical separation of U(VI) in radioactive wastewater is attracting great

* Corresponding author at: School of Public Health, Chengdu Medical College, Chengdu 610500, Sichuan, PR China.
** Corresponding author.
E-mail addresses: edwardnuclear_liu@163.com (J. Liu), zhaocs1023@163.com (C. Zhao).

https://doi.org/10.1016/j.arabjc.2024.106007
Received 13 May 2024; Received in revised form 16 September 2024; Accepted 29 September 2024
Available online 1 October 2024

attention worldwide.

Treatment methods for radioactive wastewater included sorption, chemical precipitation, ion exchange, biological treatment and membrane treatment (Li et al., 2022; Liu et al., 2019; Yuan et al., 2024). The sorption method had the advantages of low cost, easy operation, high efficiency and no secondary environmental pollution, endowed with good application prospects and development potential (Attallah et al., 2020; Elwakeel et al., 2022; Elwakeel et al., 2017; Wei et al., 2021). There are numerous studies using adsorption to remove heavy metal ions from water or to purify dye wastewater. Radioactive wastewater is usually characterized by complex composition, high acidity and salt content, and its disposal needs to be designed in an integrated manner and treated efficiently (Benettayeb et al., 2021; El-Shorbagy et al., 2021; Elgarahy et al., 2023; Elwakeel et al., 2018). A crystalline form of zirconium phosphate was firstly reported by A. Clearfield in 1964 (Clearfield et al., 1964). Due to its surface P-OH groups, layered zirconium phosphate can exchange lanthanide and actinide cations or incorporate basic molecules. In addition, zirconium phosphate has a stable layer structure, is insoluble in organic solvents and water, resistant to strong acids and alkalis of a certain strength, and has good thermal and chemical stability. As an environmentally friendly material, it is widely used in ion exchangers, sorbents, medical treatment and other fields. (Burns et al., 2012; Khan et al., 2023).

In order to meet the requirements for actual application in radioactive wastewater treatment, powder sorbents are usually processed into various shapes to achieve better efficiency (Wang et al., 2021). For example, Yang et al. found that their prepared chitosan-based hierarchical porous aerogel could be the potential uranium adsorbent because this aerogel did not show significant volume expansion after soaking in high purity water for 1 week (Yang et al., 2021). Papandreou et al. formed pellets with a diameter of 3 to 8 mm made from burnt coal fly ash and determined their performance in removing copper and cadmium ions due to their high relative porosity and excellent mechanical strength (Papandreou et al., 2007).

Considering the limited research related to the use of modified NZP for uranium sorption in radioactive wastewater and the most current experimental studies have mainly developed powdery sorbents, this has a detrimental effect on the recovery of sorbents from wastewater. In addition, most current radioactive wastewater treatment processes are equipped with column separation and synergistic membrane separation. When using powdery sorbents, there is a risk that the fluidity of the liquid phase in the system will be reduced and blockages will occur. Successful conversion of NZP into spherical sorbents is more conducive to the application in practical uranium wastewater treatment plants and the development of related processes. Polyurethane, in its molecular structure, consists of urethane bonds (–NHCOO), was a block copolymer typically prepared by the reaction of a polyester or polyether polyol with diisocyanate and was suitable as a binder due to its unique multiphase structure with soft and hard segments (Cregut et al., 2013; Magnin et al., 2020; Tai et al., 2021). Here, the porous sodium zirconium phosphate pellets (p-NZP-P) were first prepared and used for U(VI) sorption. Both static and dynamic sorption were carried out along with the real test of the wastewater for radioactive rare earth metals. The uranium sorption mechanisms were also discussed using various characterization methods such as scanning electron microscope (SEM), Transmission Electron Microscope (TEM), energy dispersive spectroscopy (EDS), X-ray diffraction spectra (XRD), Fourier transform infrared spectra (FTIR), X-ray photoelectron spectroscopy (XPS) and Brunner-Emmet-Teller (BET) analyses. The results of our work benefited research on uranium separation and enrichment in radioactive wastewater and the positive development of the nuclear industry.

2. Materials and methods

2.1. Materials

Sodium zirconium phosphate (NZP) was purchased from Resin & Zircon Technology Co., Ltd. The NZP formed by the partial exchange of sodium ions with hydrogen ions on P-OH groups of zirconium phosphate, the ions exchange reaction between sodium ions and zirconium phosphate was demonstrated in formula (1) (Clearfield et al., 1972).

$$Na^{+} + Zr(HPO_4)_2{\cdot}xH_2O \leftrightarrow Zr(NaPO_4)(HPO_4){\cdot}xH_2O + H^{+} \quad (1)$$

Other chemicals such as $UO_2(NO_3)_2{\cdot}6H_2O$, polyurethane emulsion was analytically pure reagent and used without further purification, purchased from Shanghai Aladdin Reagent Co. Besides, 1 $g{\cdot}L^{-1}$ U(VI) stock solution was obtained by dissolving 2.1093 g $UO_2(NO_3)_2{\cdot}6H_2O$ powder in pH = 2.5 acidic deionized water.

2.2. Preparation of porous sodium zirconium phosphate pellets

100 g of sodium zirconium phosphate and 70 mL of polyurethane emulsion were placed in a beaker and stirred until well mixed. The mixture was transferred to the pill making machine to obtain the cylindrical precursor with a diameter of ~3 mm and a length of ~20 cm. After cutting, polishing and vacuum drying at 70 °C for 10 h, sodium zirconium phosphate pellets with a diameter of approximately 3 mm were formed, which were named p-NZP-P after cooling to room temperature.

2.3. Characterizations and device

The detailed characterizations and device were described in Section S1 of the Supplementary Data (SD).

2.4. Static sorption experiments

30 Mg p-NZP-P were added into a flask with 25 mL different U(VI) solutions for shaking in a rotary shaker at 150 $r{\bullet}min^{-1}$. The pH of the U (VI) solutions was adjusted by adding 0.1 m NaOH and HNO_3. After uranium sorption and centrifugation at 10,000 $r{\cdot}min^{-1}$ for 4 min. The initial and equilibrium concentration of U(VI) in 1 mL supernatants were measured by the Arsenazo(III) method at 651.8 nm on a UV–Vis spectrophotometer (UV-2450, Shimadzu, Japan). The uranium sorption capacity (q_e, $mg{\cdot}g^{-1}$), sorption percentage (S, %) were separately determined by using the following formulas (2), (3)

$$q_e = \frac{(C_0 - C_e) \times V}{m} \quad (2)$$

$$S(\%) = \frac{C0 - Ce}{C0} \times 100\% \quad (3)$$

where V and m were the solutions volume (mL) and the pellets mass (mg). C_0 ($mg{\cdot}L^{-1}$) and C_e ($mg{\cdot}L^{-1}$) were the U(VI) concentration at the beginning and at equilibrium sorption, respectively.

2.5. Dynamic sorption experiments

A self-assembly column (inner diameter 10 mm, effective height 200 mm) was used for dynamic sorption experiments (Section S1 of the SD). Different amounts of p-NZP-P were filled into the column with glass wool. The p-NZP-P was completely soaked with deionized water in the column before sorption. The flow rate was controlled by the peristaltic pump and the effluents were collected every 10 min in the 5 mL centrifuge tube. The U(VI) concentration was determined using the same method as in static sorption tests.

3. Results and discussion

3.1. Characterizations and analysis

The p-NZP-P were immersed in deionized water. The results showed that p-NZP-P could maintain the shape of the spheroid after soaking for five days, as shown in Fig. 1a. The weight loss of p-NZP-P could be roughly divided into two stages (Section S2 of the SD). Stage 1: RT–350 ℃, it is associated with an approximate 22 % weight loss, caused by thermal decomposition of polyurethane to produce carbon dioxide; Stage 2: 350–800 ℃, in which nearly 5 % weight loss is due to due to the removal of water of crystallization of NZP and the condensation of its P-OH group. BET measurements (Fig. 1b) revealed that the N2 sorption–desorption curve was close to the H3-type hysteresis loop, which is commonly found in layered aggregates and mesoporous and microporous materials (Naik et al., 2010). From Fig. 1c-d, it can be seen that the volume and surface area of pores with a pore size larger than 10 nm inside the p-NZP-P decreased significantly after U(VI) sorption, which may be due to the following penetration of uranyl into this part of the pores to occupy the space. The larger volume and surface area of micropores or mesopores with a pore width of less than 10 nm after U(VI) sorption is probably due to a slight enlargement of the pores due to swelling of the p-NZP-P in solutions.

The macroscopic sizes of the p-NZP-P were displayed as pellets with a diameter of ~3 mm (Fig. 2a). The microscopic cross section of p-NZP-P is shown in Fig. 2b-f. Apparently the interior of the p-NZP-P was porous and riddled with grooves of varying depths. TEM images of the p-NZP-P showed an internal lamellar structure adhered to polyurethane (Fig. 2g-k). The characteristic peaks of Na, O, P, Zr and N appeared in the EDS spectra (Fig. 2l), indicating the combination of sodium zirconium phosphate and polyurethane component in pellets. Meanwhile, the appearance of U peak verified the U(VI) sorption ability onto the p-NZP-P in Fig. 2m.

The XRD patterns of the p-NZP-P before and after U(VI) sorption are shown in Fig. 3a. All patterns show a peak at $2\theta = \sim 26^{\circ}$, typical of Zr-Zr separation within individual layers. The NZP are defined by two additional reflections: the one at $2\theta = \sim 20^{\circ}$ corresponds to the P-P distance in the interlayer distance and the one at $2\theta = \sim 34^{\circ}$ corresponds to the P-P distance within the layer (Contreras-Ramirez et al., 2019). No sharp diffraction peaks of p-NZP-P were observed, suggesting that 1) the NZP component may have disordered and amorphous or nanocrystalline structures and 2) the presence of the polyurethane component could reduce the intensity. For U(VI)-loaded p-NZP-P, the similar broad diffraction peaks confirmed the structural stability during the sorption process (Cheng et al., 2018).

FTIR spectra are shown in Fig. 3b. The stretching and bending peaks near 3350 cm^{-1} and 1638 cm^{-1} were attributed to the –OH(H_2O) on the surfaces of materials (Zhang et al., 2008). The peaks around 3000 cm^{-1} and 1580 cm^{-1} represented the –NH and −C-N groups in polyurethane (Daud et al., 2014). The symmetric stretching shoulder peak of the P-OH functional groups was detected at 1110 cm^{-1} (Gheonea et al., 2017), along with the existence of the P-O-Zr stretching peak at around 1000 cm^{-1} (Rajeh and Szirtes, 1999). After sorption, the position and intensity of P-OH shifted by approximately 10 cm^{-1} and decreased, confirming its potential U(VI) coordination ability, accompanied by the appearance of the typical O═U═O vibration peak around 915 cm- 1 (Zeng et al., 2020).

XPS results are shown in Fig. 4. The elements C, N, O, Zr, P and Na were detected in survey spectra (Fig. 4a), which was consistent with the EDS result. The double peaks at 382.01 eV (U $4f_{7/2}$) and 392.87 eV (U $4f_{5/2}$) (Fig. 4b) suggest the sorption of hexavalent uranium on p-NZP-P (Ali, 2018). Two different peaks corresponding to P-O-Zr and P-OH at binding energies of 531.28 eV and 532.71 eV were fitted into the high-resolution (HR) O1s spectra (Fig. 4c). After U(VI) sorption, the position and abundance of P-OH decreased and shifted by about 0.25 eV, providing evidence that the P-OH participates in U(VI) sorption by p-NZP-P was involved and played a key role (Chen et al., 2021; Nakajima and Yoshida, 1996), which correlated well with the FTIR result. Notably, the positions of the fitted peaks for Na1s spectra (Fig. 4d) shifted significantly, illustrating the possible ion exchange reaction between Na + and U(VI) involved in sorption (Buvaneswari et al., 2004; Naik et al., 2004). The HR spectra of Zr3d and P2p (Fig. 4e-f) hardly changed after U(VI) sorption, it could be concluded that Zr and P elements did not directly contribute to the sorption process.

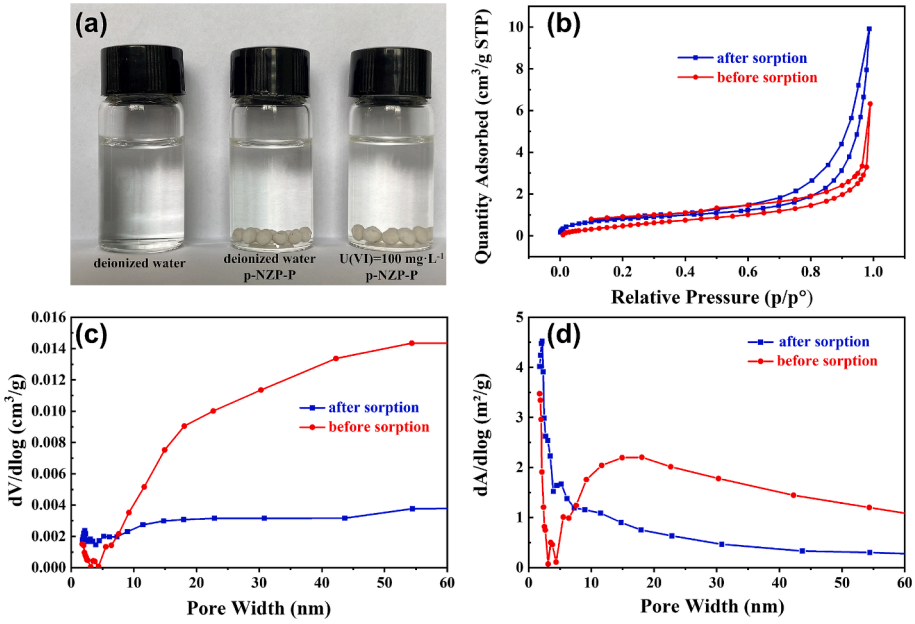

Fig. 1. (a) The exterior of p-NZP-P after soaking in solutions for five days, (b) BET measurement of p-NZP-P, (c) dV/dlog pore volume and (d) dA/dlog pore area before and after sorption.

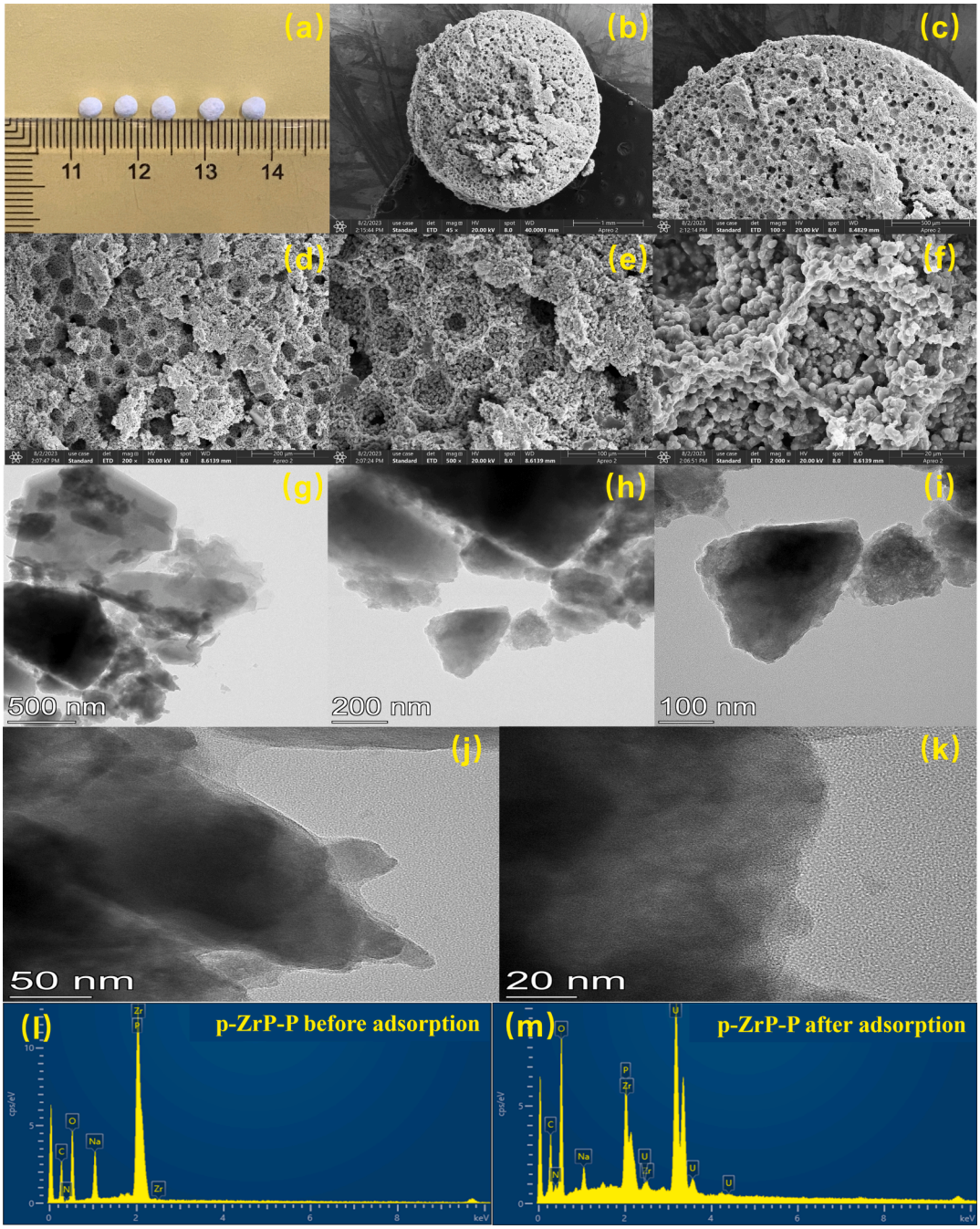

Fig. 2. (a) p-NZP-P, (b-f) SEM images of p-NZP-P and (g-k) TEM images of p-NZP-P. EDS images of p-NZP-P (l) before and (m) after U(VI) sorption.

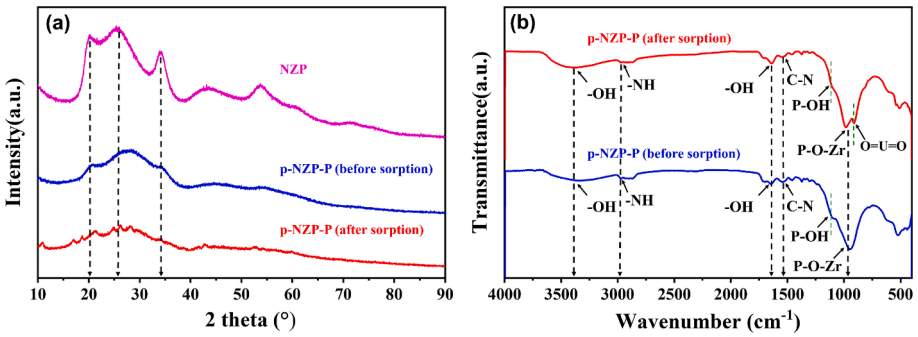

Fig. 3. (a) XRD patterns, (b) FT-IR spectra of NZP and p-NZP-P before and after sorption.

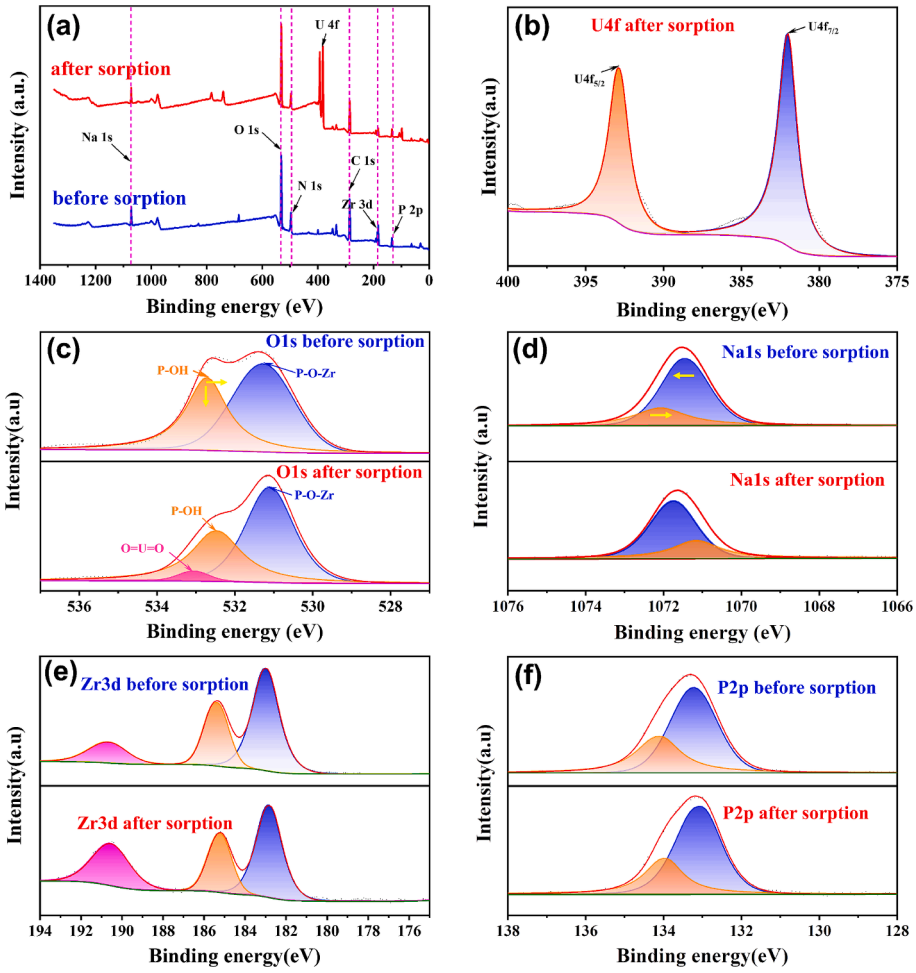

Fig. 4. (a) XPS spectra of p-NZP-P before and after sorption, (b) U 4f, (c) O 1 s, (d) Zr 3d, (e) Na 1 s, (f) P 2p HR spectra of p-NZP-P before and after sorption.

3.2. Effect of key factors in static sorption

3.2.1. Effects of contact time and sorption kinetics

Contact time was a significant factor in the U(VI) sorption kinetics of sorbents. More than 70 % uranium was removed and the sorption capacity reached ~74.8 mg·g^{-1} with an equilibrium time of ~1100 min (Fig. 5a). Pseudo-first-order, pseudo-second-order, and intraparticle diffusion kinetics models were used herein, and their equations and corresponding parameters were shown and listed in Section S3 of the SD. The intraparticle diffusion models clearly described the sorption data better (Fig. 5b-d) and proved that U(VI) continuously diffused inward and occupied the sorption sites within the p-NZP-P until the sorption equilibrium was reached (Liu et al., 2021).

3.2.2. Effects of initial U(VI) concentration and sorption isotherms

It was found that the sorption capacity increased as the initial U(VI) concentration increased from 100 mg·L^{-1} to 300 mg·L^{-1}, the sorption capacity of U(VI) was greater at higher temperatures in all $[U(VI)]_{initial}$ conditions (Fig. 6a). The isothermal models were fitted in Fig. 6b, and the Section S4 of the SD showed the corresponding parameters. All high R^2 values of the two models indicated that homogeneous and heterogeneous sorption processes occurred simultaneously. Furthermore, the theoretical maximum q_m calculated from the Langmuir model was ~199.78 mg·g^{-1} at a temperature of 298 K, indicating a remarkable U (VI) sorption capacity of p-NZP-P.

3.2.3. Effects of temperature and sorption thermodynamic

In Fig. 7a, it is shown that increasing the temperature promoted U (VI) sorption due to the enhancement of intermolecular motion. Fig. 7b is the thermodynamic fitting of U(VI) sorption by p-NZP-P with detailed parameters in Section S5 of the SD. As can be seen, the positive ΔH^{θ} and ΔS^{θ} indicated that the sorption of U(VI) by p-NZP-P was an endothermic and randomness-enhancing process. Furthermore, the values of ΔG^{θ} were negative and decreased with increasing temperature, indicating that the sorption process occurred spontaneously and favorably at higher temperatures.

3.2.4. Effects of initial pH

Fig. 8a shows that the increase in initial pH from 2.5 to 4.5 resulted in an increase in q_e due to the decreasing surface protonation of p-NZP-P and the changes in sepecies of U(VI). While a decrease in q_e was observed, when the initial pH exceeded 4.5. The species of U(VI) include UO_2^{2+}, UO_2OH^{+}, $(UO_2)_2(OH)_2^{2+}$, $(UO_2)_3(OH)_5^{+}$, $(UO_2)_3(OH)_4^{2+}$ and $(UO_2)_4(OH)_7^{2+}$ (Fig. 8b). The experimental results were also confirmed by the zeta potentials. It can be seen that the surface of the p-NZP-P is positively charged when the $pH_{initial}$ is less than ~3.16 and negatively charged when the $pH_{initial}$ is greater than ~3.16 (Section S6 of the SD). The species of U(VI) in the solution is mainly UO_2^{2+} when the $pH_{initial}$ is between 2.5 and 3, which is electrostatically repelled by the p-NZP-P, resulting in lower sorption of U(VI). When the $pH_{initial}$ is between 3 and 4.5, the species of U(VI) is converted from UO_2^{2+} to UO_2OH^{+}, $(UO_2)_2(OH)_2^{2+}$ and $(UO_2)_3(OH)_4^{2+}$, resulting in higher sorption of U(VI) due to electrostatic attraction. However, when the $pH_{initial}$ was greater than 4.5, although the negative charge on the surface of the p-NZP-P was still increasing, the species of U(VI) is converted from UO_2^{2+}, UO_2OH^{+}, $(UO_2)_2(OH)_2^{2+}$, $(UO_2)_3(OH)_4^{2+}$ to $(UO_2)_3(OH)_5^{+}$, and $(UO_2)_4(OH)_7^{+}$, the

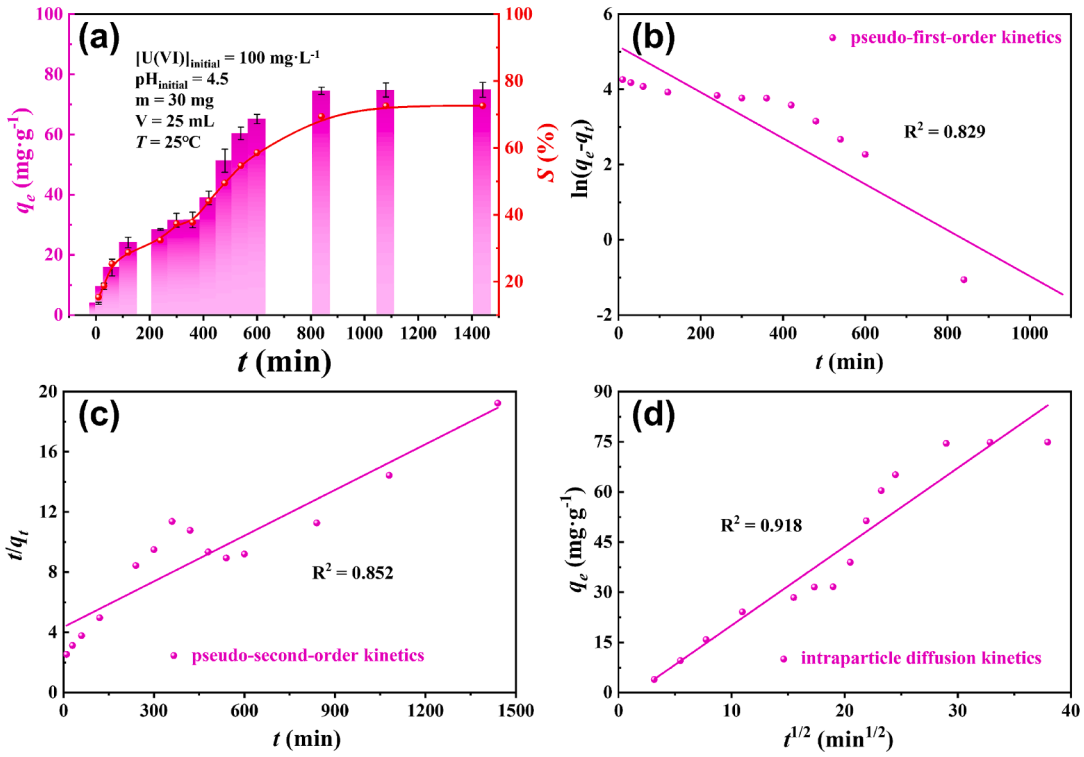

Fig. 5. U(VI) sorption by p-NZP-P: (a) effect of contact time and (b-d) kinetics models (m = 30 mg, V = 25 mL, pH = 4.5, $[U(VI)]_{initial}$ = 100 mg·L^{-1}, T = 25 °C).

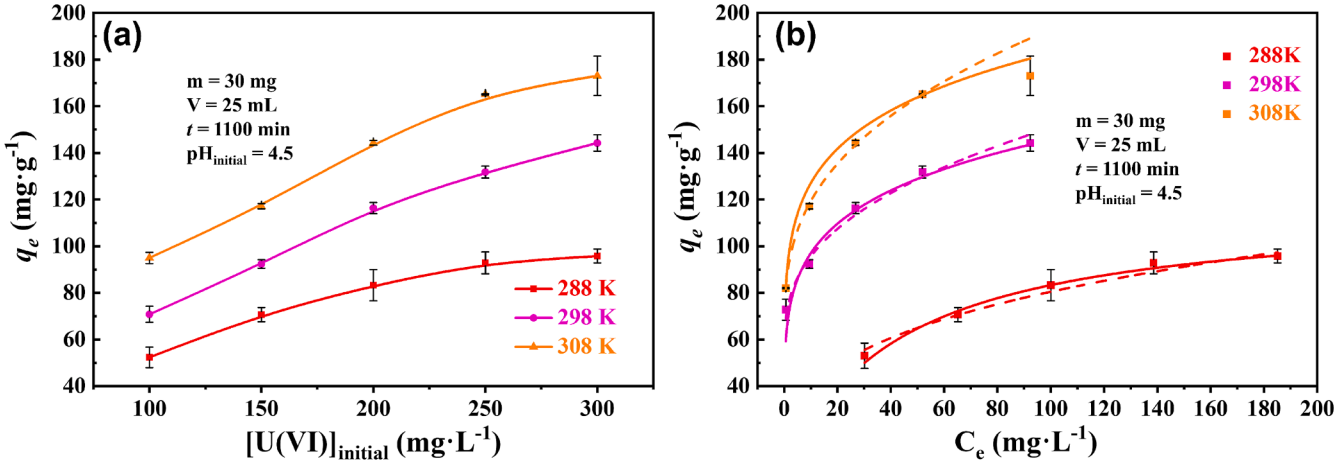

Fig. 6. U(VI) sorption by p-NZP-P: (a) effect of initial U(VI) concentration in different temperature (m = 30 mg, V = 25 mL, t = 1100 min, $pH_{initial}$ = 4.5) and (b) sorption isotherms (solid line is Langmuir model, dotted line is Freundlich model).

total positive charge of the uranyl in the solution was reduced, therefore the electrostatic attraction between uranyl and p-NZP-P was slightly reduced. This results in a slight decrease in U(VI) sorption. Nonetheless, p-NZP-P exhibited a high U(VI) sorption capacity of ~77.5 mg·g^{-1} at pH = 4.5, T = 25 ℃ and $[U(VI)]_{initial}$ = 100 mg·g^{-1}.

The equilibrium pH ($pH_{equilibrium}$) after U(VI) sorption is displayed in Fig. 8c. For $pH_{initial}$ 4.5 and 5.5, the changes in $pH_{equilibrium}$ are within the limited range, showing small fluctuations. Fig. 8d shows the absolute value of the difference (|ΔpH|) between $pH_{equilibrium}$ and $pH_{initial}$. Clearly, at $pH_{initial}$ 4.5 ~ 5.5, the change of solution pH before and after sorption is relatively small (≤ 0.25), which has little impact on the study of U(VI) sorption by p-NZP-P in aqueous solutions.

3.3. *Effect of key factors on dynamic sorption and Tomas model*

The effect of key factors on dynamic U(VI) sorption by p-NZP-P is shown in Fig. 9. Taking measurement errors into account, we defined that 10 % and 90 % of the initial U(VI) concentration represented breakthrough and saturation times, respectively. Apparently, with the increase in p-NZP-P mass, both the breakthrough and saturation points were delayed (Fig. 9a), as larger amounts of p-NZP-P provided more U (VI) sorption sites to increase the contact time extend and probability between the uranyl and the pellets. Accordingly, the breakthrough time (t_b) were ~77.5 min (0.5 g), 148.8 min (1 g) and 213.8 min (2 g), while the saturation point time (t_e) was 446.8 min, 526.9 min and 639.7 min, respectively.

The influence of the flow rate is shown in Fig. 9b. Both the breakthrough and saturation times were advanced in higher flow rate. It is

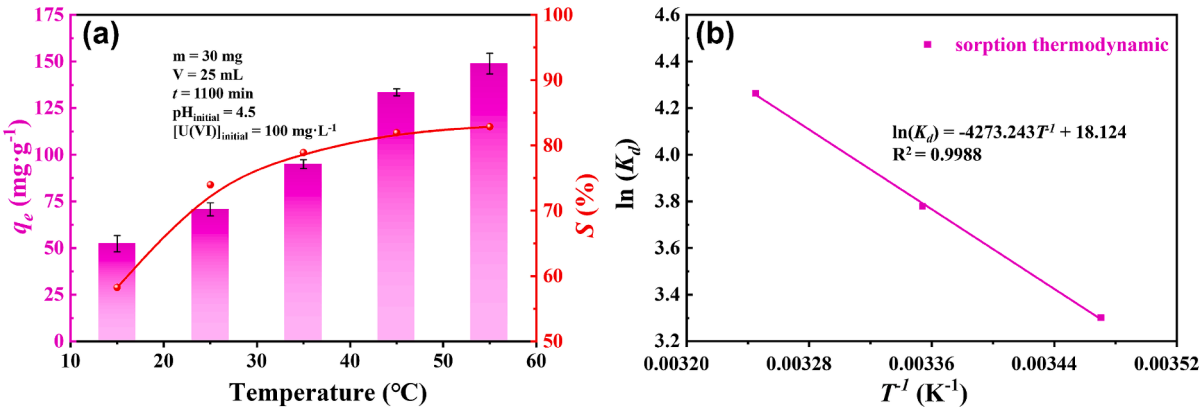

Fig. 7. U(VI) sorption by p-NZP-P: (a) effect of temperature and (b) thermodynamic (m = 30 mg, V = 25 mL, t = 1100 min, $pH_{initial}$ = 4.5, $[U(VI)]_{initial}$ = 100 mg·L^{-1}).

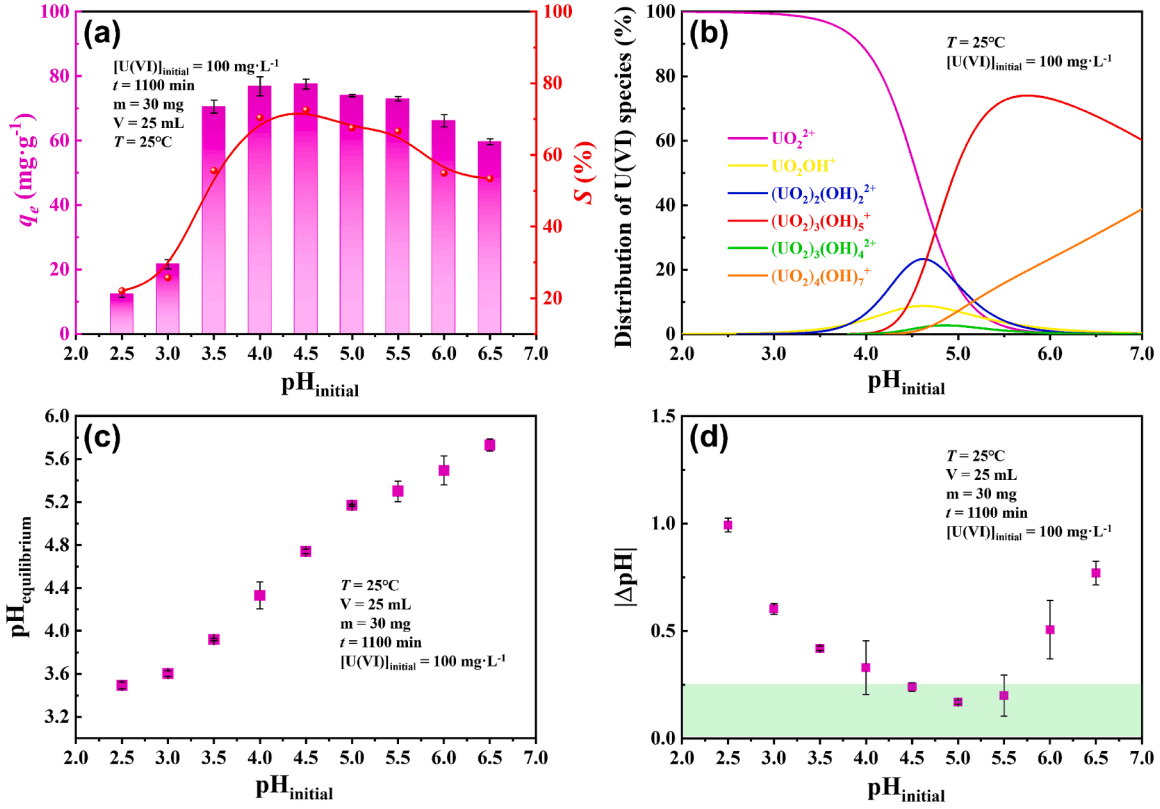

Fig. 8. Effect of (a) initial pH on the sorption of U(VI) by p-NZP-P, (b) Distribution of U(VI) species at different pH values, (c) $pH_{equilibrium}$ and (d) |ΔpH| after U(VI) sorption by p-NZP-P in aqueous solution.

predictable that at high flow rate, the uranyl in the solutions lacked enough time to diffuse into the interior of the p-NZP-P, resulting in low removal efficiency during the dynamic U(VI) sorption process.

The advanced breakthrough and saturation time were observed in Fig. 9c at high initial U(VI) concentration because the accelerated mass transfer rate satisfied the rapid occupancy of U(VI) for the sorption sites. In other words, the amount of available sorption sites was limited while the sorbent mass was constant, resulting in a reduction in the overall removal efficiency.

The breakthrough and saturation times of dynamic U(VI) sorption by p-NZP-P at different pH values are shown in Fig. 9d. Compared to the breakthrough and saturation times at pH = 3.5 and 5.5, the longest time points of ~148.8 min and ~526.9 min occurred at pH = 4.5, reflecting the relatively high dynamic sorption capacity of U(VI). This result correlated well with that in the static sorption experiment.

For dynamic sorption data analysis and calculation of saturation sorption capacity and rate constant, the Thomas model, an idealized model that does not assume axial diffusion, was used. His equation was shown as follows.

$$Ct/C0 = 1/[1 + \exp(KThq0m/Q - KThC0t)] \quad (4)$$

Where K_{th} was the rate constant of the Thomas model (mL·min^{-1}·mg^{-1}). q_0 was the predicted dynamic saturated sorption density (mg·g^{-1}). C_0 and C_t were the initial U(VI) concentration and the concentration of uranium after t minutes, respectively (mg·L^{-1}). m was the mass of the p-NZP-P (g). Q was the flow rate of the solution in the peristaltic pump (mL·min^{-1}). t was the system running time (min).

The fitting curves and detailed parameters are shown in Fig. 10 and

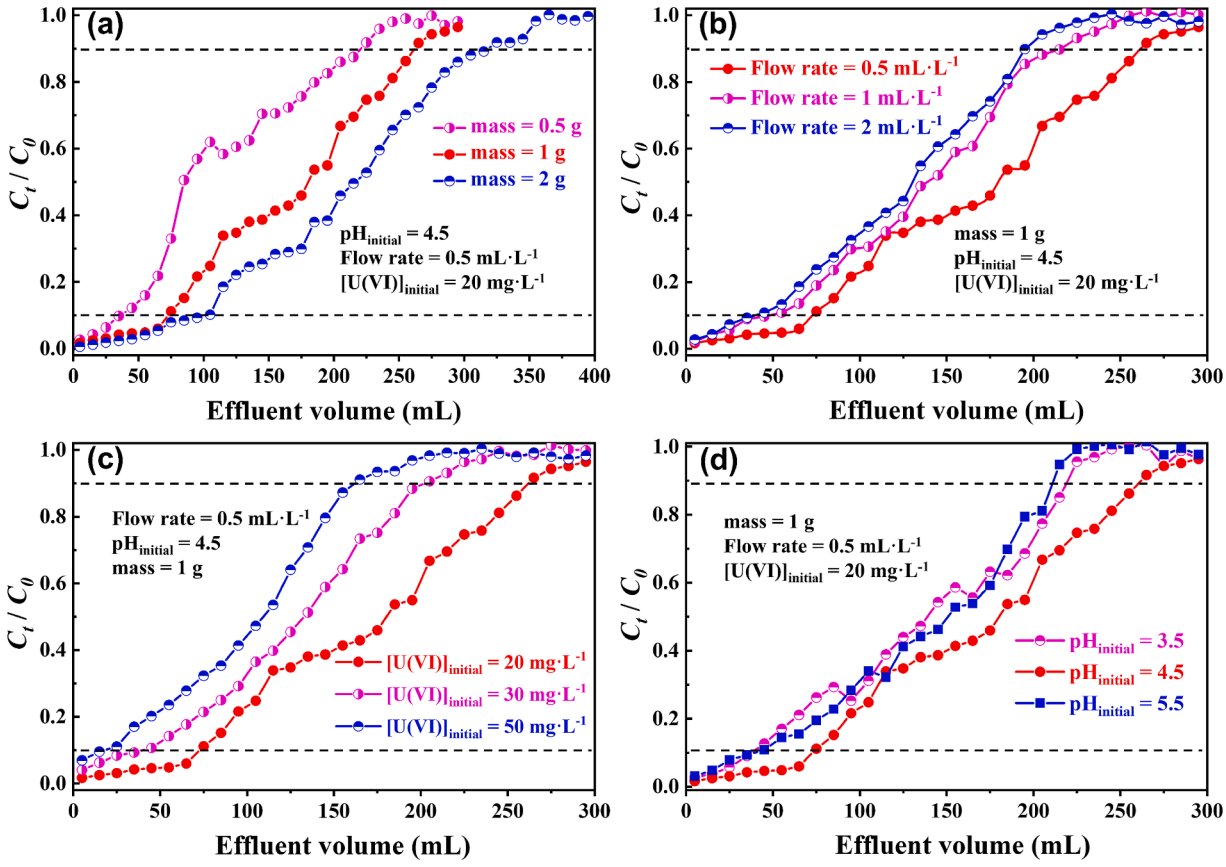

Fig. 9. Effect of (a) mass, (b) flow rate, (c) initial U(VI) concentration, (d) initial pH on U(VI) dynamic sorption by p-NZP-P.

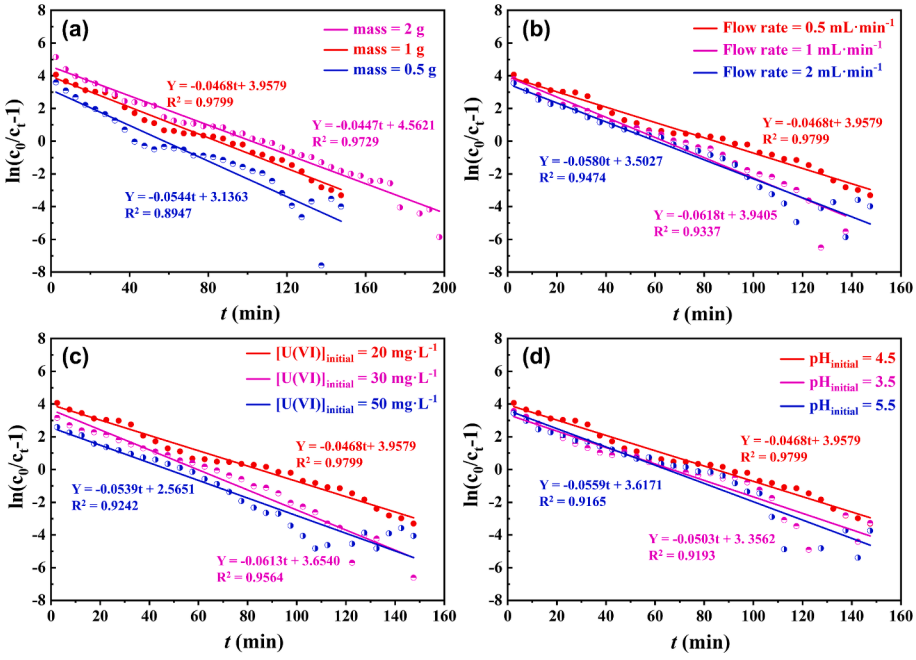

Fig. 10. The fitting curves of Tomas models for the U(VI) sorption on different conditions: (a) mass, (b) flow rate, (c) initial U(VI) concentration, (d) initial pH.

Section S7 of the SD. The results showed that the Thomas model can describe the dynamic sorption process well. K_{Th} decreased while the mass of p-NZP-P increased, confirming the increasing amounts of active sorption sites and the improvement in removal efficiency corresponding to the advancement of breakthrough and saturation time. However, K_{Th} increased at the fast flow rate and high initial U(VI) concentration, which was consistent with the dynamic sorption result. The increase in the q_o was related to the improvement in sorbent utilization when decreasing the p-NZP-P mass or increasing the flow rate and initial U(VI) concentration.

3.4. Radioactive rare earth wastewater treatment and effects of coexisting ions

The sources of uranium in water bodies primarily include uranium mining, smelting and processing of uranium, uranium leaks due to unusual accidents in nuclear power plants, the production and testing of nuclear weapons, and the use of weapons with depleted uranium. Wastewater production from uranium mines varies over a wide range, with U(VI) concentrations ranging from 0.18 to 4 mg·L^{-1}. Collection of rare earth wastewater from a tailings pond in southwest Sichuan, China. The recirculation device (Section S1 of the SD) was used for the U(VI) removal test from radioactive rare earth wastewater. The recirculation device (Section S1 of the SD) was used for the U(VI) removal test from radioactive rare earth wastewater. The column was filled with 2 g of p-NZP-P and the volume of the radioactive rare earth wastewater in the mother liquor tank was 500 ml. The flow rate of the recirculation device was set to ~3 L/h. The U(VI) concentration in the water draining into the eluent tank was measured by ICP-MS, and a significant decrease (~81.7 %) in the U(VI) concentration could be achieved after 1 h of recirculation treatment (Fig. S5 in Section S8 of the SD).

The effects of coexisting ions on U(VI) sorption by p-NZP-P when C_0 = 100 mg·L^{-1} for all cations, m = 30 mg, pH = 4.5, t = 1100 min, T = 25 ℃ and V = 25 mL were evaluated in Fig. S6 (Section S8 of the SD). The results showed that the removal of U(VI) by p-NZP-P could still reach ~68.87 % in a solution where multiple cations were present at the same time. It also reaffirms the potential of p-NZP-P to remove uranium from radioactive wastewater.

3.5. Desorption and reusability

The regenerative property of p-NZP-P is one of the most important elements to measure its application potential. The aim of the desorption experiments was to evaluate the potential of p-NZP-P for practical U(VI) recovery. The U(VI)-loaded p-NZP-P in aqueous solution was desorbed by different desorbents (HNO_3, H_2SO_4, HCl, $NaHCO_3$, NaCl and NaOH), with an equal concentration of 0.1 mol·L^{-1}. From Fig. 11a, it can be seen that the highest desorption rate with 0.1 mol·L^{-1} HCl was 82.36 %. The results of the reusability experiments are shown in Fig. 11b. The 25 mL of 0.1 mol·L^{-1} HCl solutions were used to repeat the sorption elution five times. The sorption capacity of p-NZP-P for U(VI) only decreased by ~12.6 % after 5 cycles of repeated use, indicating the stable chemical properties and excellent recycling performance of p-NZP-P.

The sorption capacities of other materials are compared in Table 1. Compared with other materials, our synthesized material has excellent sorption performance among spherical sorbents. The sorption ability of the p-NZP-P is not sufficiently advantageous compared to the many materials. however, most studies have not focused on the suitability of sorbents for use in practical processes for treating radioactive wastewater, traditional powdery sorbents tend to clog the treatment device's piping or filter membrane and are more difficult to recover from solutions. In summary, p-NZP-P is more suitable for practical radioactive

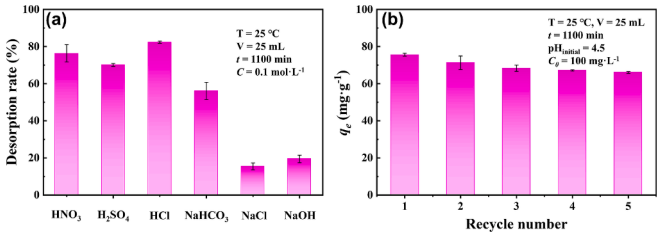

Fig. 11. The U(VI)-loaded p-NZP-P in aqueous solution was desorbed by different desorbents with an equal concentration of 0.1 mol·L^{-1}, respectively (T = 25 ℃, V: 25 mL, t: 1100 min, C = 0.1 mol·L^{-1}) and (b) the reusability experiments of U(VI) sorption on p-NZP-P (T = 25 ℃, $pH_{initial}$ = 4.5, V = 25 mL, C_0 = 100 mg·L^{-1}, t = 1100 min).

Table 1
Comparison of sorption capacity for different nuclide with various sorbents.

Sorbent	Appearance	pH	q_e	Ref.
AC-Q	powder	4.7	~63 mg·g^{-1}	(Elashry et al., 2022)
Fe_3O_4/GO	powder	5.5	~69.5 mg·g^{-1}	(Zong et al., 2013)
15 % PMo12/UiO-66	powder	5.5	~131.4 mg·g^{-1}	(Zhang et al., 2022a)
CS-PTA-DMAs	aerogel	6	~160 mg·g^{-1}	(Yang et al., 2021)
PGG@C	powder	4	~0.5 mmol·g^{-1}	(Hamza et al., 2021)
UR/SiO_2	powder	5	~0.6 mmol·g^{-1}	(Hamza et al., 2022)
TEPA@MCHS	powder	4	~1.8 mmol·g^{-1}	(Elwakeel et al., 2014)
Schiff's base magnetic chitosan composite	powder	4	~2.3 mmol·g^{-1}	(Elwakeel and Atia, 2014)
p-NZP-P	pellet	4.5	~77.5 mg·g^{-1}	This work

wastewater treatment processes, and in the current study, p-NZP-P has a higher sorption capacity for U(VI) in the spherical sorbents.

3.6. Sorption mechanisms

In particular, the likely mechanisms of U(VI) sorption by p-NZP-P from aqueous solutions were schematically presented in Fig. 12. The decrease in the relative abundance of surface –OH groups after U(VI) sorption indicated that the hydroxyl groups on NZP (P–OH) played a key role in U(VI) sorption by p-NZP-P U(VI) solutions. Furthermore, the shift of Na1s peaks suggests that the ion exchange reaction of Na^+ with uranyl in the NZP interlayer also contributes to U(VI) sorption by p-NZP-P (Yuan et al., 2024). The component of polyurethane in p-NZP-P was very stable as the binder before and after the sorption and did not participate in the sorption process (Zhang et al., 2022b). A variety of characterization results and experimental phenomena support the above assumption about the sorption mechanism.

4. Conclusions

In this work, the novel porous sodium zirconium phosphate pellets (p-NZP-P) were first prepared to adsorb uranium from aqueous solution. After soaking for five days, p-NZP-P showed excellent macroscopic stability. The characterization verified the porous microstructure of the sorbent and the structural stability during the U(VI) sorption process. And the sorption mechanisms were suggested to be involved in –OH coordination and ion exchange.

The results of the static sorption experiment showed that the U(VI) sorption capacity of 77.5 ± 1.5 mg·g^{-1} could be recovered by p-NZP-P when the initial concentration of U(VI) was 100 mg/ L, pH = 4.5, T = 25 ℃, m = 30 mg and V = 25 mL. Kinetics and thermodynamics suggested that intraparticle diffusion and a spontaneous endothermic process occurred. Furthermore, the theoretical maximum qm calculated from the Langmuir model was ~199.9 mg·g^{-1}, indicating a remarkable U(VI) sorption capacity of p-NZP-P. Based on the results of the dynamic sorption experiments, the increase in mass and the decrease in the initial U(VI) concentration and flow rate delayed the breakthrough and saturation times at pH 4.5. The Thomas model revealed that increasing the p-NZP-P mass or decreasing the flow rate and initial U(VI) concentration resulted in a decrease in K_{Th}, corresponding to the breakthrough delay and saturation time. Furthermore, the increase in the q_o value related to the increasing utilization of our pellets while decreasing the mass or increasing the flow rate and initial U(VI) concentration. Radioactive rare earth wastewater treatment results suggested that p-NZP-P could be the potential uranium sorbent due to its good stability and efficiency. Repeatability experiments showed that the sorption capacity of p-NZP-P

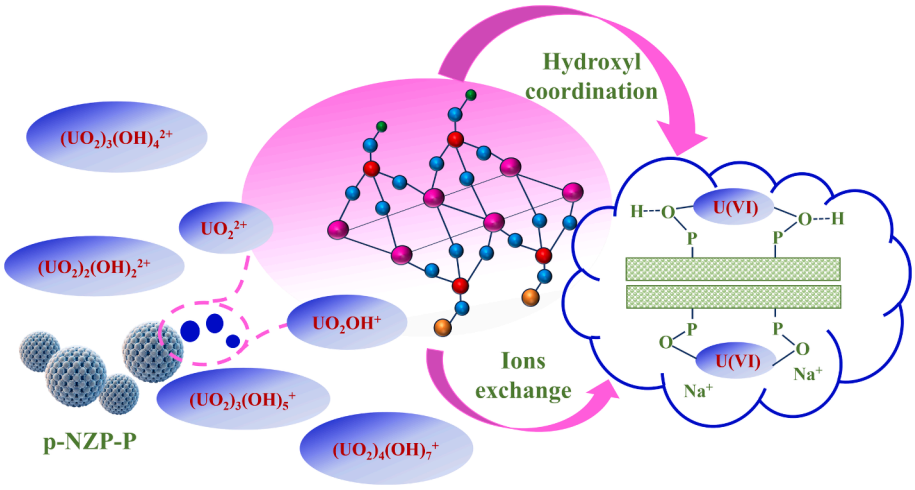

Fig. 12. Probable mechanisms of U(VI) sorption by p-NZP-P in aqueous solution.

for U(VI) only decreased by ~12.6 % after 5 cycles of repeated use, indicating the stable chemical properties and excellent recycling performance of p-NZP-P. Mechanistic analyzes showed that the sorption capacity of p-NZP-P is mainly due to –OH coordination and Na^+ exchange.

Our article verified the technical application potentials of p-NZP-P and provided references for the development of practical materials for uranium removal from radioactive wastewater.

CRediT authorship contribution statement

Cheng Wang: Writing – original draft, Methodology, Investigation, Data curation, Conceptualization. **Bingtao Gui:** Validation, Formal analysis. **Tianjie Li:** Validation, Methodology. **Ruiyang Chang:** Investigation, Formal analysis. **Junxiang Shu:** Methodology, Formal analysis. **Xiaoqin Deng:** Resources, Funding acquisition. **Li Chen:** Formal analysis. **Maodan Luo:** Formal analysis. **Bing Jiang:** Formal analysis. **Su Xu:** Formal analysis. **Juan Zhai:** Methodology, Investigation, Formal analysis. **Jun Liu:** Writing – review & editing, Supervision, Methodology, Funding acquisition, Conceptualization. **Changsong Zhao:** Funding acquisition, Project administration.

Declaration of Competing Interest

The authors declare that they have no known competing financial interests or personal relationships that could have appeared to influence the work reported in this paper.

Acknowledgments

This work was supported by the National Natural Science Foundation of China (42107233, 22006004), the CMC Excellent-talent Program (2024yxGzn07), the Natural Science Foundation of Sichuan Province (2022NSFSC1225), the Ecological Environment Protection Technology Project Plan of Sichuan Province (2023HB06), and the Open Project of High Level Public Health College (grant no. XMUCMC202404).

Appendix A. Supplementary data

Supplementary data to this article can be found online at https://doi.org/10.1016/j.arabjc.2024.106007.

References

Ali, A.H., 2018. Potentiality of zirconium phosphate synthesized from zircon mineral for uptaking uranium. Sep. Sci. Technol. 53 (14), 2284–2296. https://doi.org/10.1080/01496395.2018.1445115.

Attallah, M.F., Hilal, M.A., Moussa, S.I., 2017. Quantification of some elements of nuclear and industrial interest from zircon mineral using neutron activation analysis and passive gamma-ray spectroscopy. Appl. Radiat. Isot. 128, 224–230. https://doi.org/10.1016/j.apradiso.2017.07.018.

Attallah, M.F., Youssef, M.A., Imam, D.M., 2020. Preparation of novel nano composite materials from biomass waste and their sorptive characteristics for certain radionuclides. Radiochim. Acta 108 (2), 137–149. https://doi.org/10.1515/ract-2019-3108.

Attallah, M.F., Elchine, D., Grödler, D., Margreiter, R., Maslo, M., Michel, M., Jon, P.O., Strub, E., Döllen, S.V., 2024. Trace-scale extraction of carrier-free tungsten radioisotope as a homolog of Sg using ionic liquid from acid solutions: Kinetic study. Sep. Purif. Technol. 331, 125418. https://doi.org/10.1016/j.seppur.2023.125418.

Benettayeb, A., Morsli, A., Elwakeel, K.Z., Hamza, M.E., Guibal, E., 2021. Recovery of Heavy Metal Ions Using Magnetic Glycine-Modified Chitosan-Application to Aqueous Solutions and Tailing Leachate. Appl. Sci. Basel. 11 (18). https://doi.org/10.3390/app11188377.

Burns, J.D., Clearfield, A., Borkowski, M., Reed, D.T., 2012. Pillared metal(IV) phosphate phosphonate extraction of actinides. Radiochim. Acta. 100 (6), 381–387. https://doi.org/10.1524/ract.2012.1929.

Buvaneswari, G., Kutty, K.V.G., Varadaraju, U.V., 2004. Thermal expansion behaviour of sodium zirconium phosphate structure type phosphates containing tin. Mater. Res. Bull. 39 (3), 475–488. https://doi.org/10.1016/j.materresbull.2003.10.015.

Chen, L., Wang, H., Cao, X., Feng, Y., Zhang, Z., Wang, Y., Liu, Y., 2021. Effects of different phosphorus sources on the adsorption of U(VI) by Zr(IV) organophosphate hybrids. J. Solid State Chem. 302. https://doi.org/10.1016/j.jssc.2021.122434.

Cheng, Y., Wang, X.D., Jaenicke, S., Chuah, G.K., 2018. Mechanochemistry-Based Synthesis of Highly Crystalline γ-Zirconium Phosphate for Selective Ion Exchange. Inorg. Chem. 57 (8), 4370–4378. https://doi.org/10.1021/acs.inorgchem.7b03202.

Clearfield, A., Oskarsson, A., Oskarsson, C., 1972. On the mechanism of ion exchange in crystalline zirconium phosphates. VI. The effect of crystallinity of the exchanger on Na+/H+ exchange. Ion Exch. Membr. 1 (2), 91–107.

Clearfield, A., Stynes, J.A., 1964. The preparation of crystalline zirconium phosphate and some observations on its ion exchange behaviour. J. Inorg. Nucl. Chem. 26 (1), 117–129. https://doi.org/10.1016/0022-1902(64)80238-4.

Contreras-Ramirez, A., Tao, S., Day, G.S., Bakhmutov, V.I., Billinge, S.J.L., Zhou, H.C., 2019. Zirconium Phosphate: The Pathway from Turbostratic Disorder to Crystallinity. Inorg. Chem. 58 (20), 14260–14274. https://doi.org/10.1021/acs.inorgchem.9b02442.

Cregut, M., Bedas, M., Durand, M.J., Thouand, G., 2013. New insights into polyurethane biodegradation and realistic prospects for the development of a sustainable waste recycling process. Biotechnol. Adv. 31 (8), 1634–1647. https://doi.org/10.1016/j.biotechadv.2013.08.011.

Daud, F.N., Ahmad, A., Badri, K.H., 2014. An Investigation on the Properties of Palm-Based Polyurethane Solid Polymer Electrolyte. Int. J. Polym. Sci. DOI: 10.1155/2014/326716.

Elgarahy, A.M., Maged, A., Elwakeel, K.Z., El-Gohary, F., El-Qelish, M., 2023. Tuning cationic/anionic dyes sorption from aqueous solution onto green algal biomass for biohydrogen production. Environ. Res. 216, 1–14. https://doi.org/10.1016/j.envres.2022.114522.

El-Shorbagy, H.G., El-Kousy, S.M., Elwakeel, K.Z., Abd El-Ghaffar, M.A., 2021. Eco-friendly Chitosan Condensation Adduct Resins for Removal of Toxic Silver Ions from Aqueous Medium. J. Ind. Eng. Chem. 100, 410–421. https://doi.org/10.1016/j.jiec.2021.04.029.

Elwakeel, K.Z., Ahmed, M.M., Akhdhar, A., Sulaiman, M.G.M., Khan, Z.A., 2022. Recent advances in alginate-based adsorbents for heavy metal retention from water: a review. Desalin. Water Treat. 272, 50–74. https://doi.org/10.5004/dwt.2022.28834.

Elwakeel, K.Z., Atia, A.A., 2014. Uptake of U(VI) from aqueous media by magnetic Schiff's base chitosan composite. J. Cleaner Prod. 70, 292–302. https://doi.org/10.1016/j.jclepro.2014.02.017.

Elwakeel, K.Z., Atia, A.A., Guibal, E., 2014. Fast removal of uranium from aqueous solutions using tetraethylenepentamine modified magnetic chitosan resin. Bioresour. Technol. 160, 107–114. https://doi.org/10.1016/j.biortech.2014.01.037.

Elwakeel, K.Z., El-Bindary, A.A., Kouta, E.Y., 2017. Retention of copper, cadmium and lead from water by Na-Y-Zeolite confined in methyl methacrylate shell. J. Environ. Chem. Eng. 5 (4), 3698–3710. https://doi.org/10.1016/j.jece.2017.06.049.

Elwakeel, K.Z., El-Bindary, A.A., Kouta, E.Y., Guibal, E., 2018. Functionalization of polyacrylonitrile/Na-Y-zeolite composite with amidoxime groups for the sorption of Cu(II), Cd(II) and Pb(II) metal ions. Chem. Eng. J. 332, 727–736. https://doi.org/10.1016/j.cej.2017.09.091.

Gheonea, R., Crasmareanu, E.C., Plesu, N., Sauca, S., Simulescu, V., Ilia, G., 2017. New Hybrid Materials Synthesized with Different Dyes by Sol-Gel Method. Adv. Mater. Sci. Eng. https://doi.org/10.1155/2017/4537039.

Hamza, M.F., Fouda, A., Elwakeel, K.Z., Wei, Y., Guibal, E., Hamad, N.A., 2021. Phosphorylation of Guar Gum/Magnetite/Chitosan Nanocomposites for Uranium (VI) Sorption and Antibacterial Applications. Mol. 26 (7), 1920. https://doi.org/10.3390/molecules26071920.

Hamza, M.F., Wei, Y., Khalafalla, M.S., Abed, N.S., Fouda, A., Elwakeel, K.Z., Eric, G., Hamad, N.A., 2022. U(VI) and Th(IV) recovery using silica beads functionalized with urea- or thiourea-based polymers – Application to ore leachate. Sci. Total Environ. 821, 153184. https://doi.org/10.1016/j.scitotenv.2022.153184.

Haneklaus, N., 2021. Unconventional Uranium Resources From Phosphates. Encyclopedia of Nuclear Energy. 286–291. https://doi.org/10.1016/B978-0-12-819725-7.00152-5.

Khan, U., Zaib, A., Ishak, A., Eldin, S.M., Alotaibi, A.M., Raizah, Z., Waini, I., Elattar, S., Abed, A.M., 2023. Features of hybridized AA7072 and AA7075 alloys nanomaterials with melting heat transfer past a movable cylinder with Thompson and Troian slip effect. Arabian J. Chem. 16 (2). https://doi.org/10.1016/j.arabjc.2022.104503.

Li, J., Li, Y., Cui, K., Li, H., Feng, J., Pu, X., Xiong, W., Liu, N., Yuan, G., 2022. Novel MOFs-based ion-imprinted polymer for selective separation of cobalt ions from waste battery leaching solution. Inorg. Chim. Acta. 536. https://doi.org/10.1016/j.ica.2022.120922.

Liu, H., Mao, Y., 2021. Graphene oxide-based nanomaterials for uranium adsorptive uptake. ES Mater. Manuf. 13, 3–22. https://doi.org/10.30919/esmm5f453.

Liu, J., Zhao, C., Wang, J., He, H., Yuan, G., Wang, H., Yang, J., Liao, J., Yang, Y., Liu, N., 2019. Adsorption of U(VI) from eutrophic aquesous solutions in a U(VI)-P-CO3 system with hydrous titanium dioxide supported by polyacrylonitrile fiber. Hydrometallurgy. 183, 29–37. https://doi.org/10.1016/j.hydromet.2018.11.009.

Ma, H., Shen, M., Tong, Y., Wang, X., 2023. Radioactive Wastewater Treatment Technologies. A Review. Mol. 28 (4). https://doi.org/10.3390/molecules28041935.

Magnin, A., Pollet, E., Phalip, V., Averous, L., 2020. Evaluation of biological degradation of polyurethanes. Biotechnol. Adv. 39. https://doi.org/10.1016/j.biotechadv.2019.107457.

Naik, A.H., Thakkar, N.V., Dharwadkar, S.R., Mudher, K.D.S., Venugopal, V., 2004. Microwave assisted low temperature synthesis of sodium zirconium phosphate (NaZr2P3O12). J. Therm. Anal. Calorim. 78 (3), 707–713. https://doi.org/10.1007/s10973-005-0436-0.

Naik, A.H., Deb, S.B., Chalke, A.B., Saxena, M.K., Ramakumar, K.L., Venugopal, V., Dharwadkar, S.R., 2010. Microwave-assisted low temperature synthesis of sodium zirconium phosphate (NZP) and the leachability of some selected fission products incorporated in its structure - A case study of leachability of cesium. J. Chem. Sci. 122 (1), 71–82. https://doi.org/10.1007/s12039-010-0009-8.

Nakajima, Y., Yoshida, I., 1996. Sodium selective ion-exchange properties of zirconium phosphate, HZr2(PO4)3, and its application for the removal of sodium ions. Anal. Sci. 12 (6), 935–940. https://doi.org/10.2116/analsci.12.935.

Papandreou, A., Stournaras, C.J., Panias, D., 2007. Copper and cadmium adsorption on pellets made from fired coal fly ash. J. Hazard. Mater. 148 (3), 538–547. https://doi.org/10.1016/j.jhazmat.2007.03.020.

Pei, H., Dong, Z., Li, Z., Huang, J., Jiang, Y., Li, Z., Xu, L., Cao, X., Liu, Y., Zhang, Z., Yang, G., 2024. Synergistic effect of homojunction and Ohmic junctions in CdS boosting spatial charge separation for U(VI) photoreduction. 1-11. Nano Res. DOI: 10.1007/s12274-024-6637-y.

Rajeh, A.O., Szirtes, L., 1999. FT-IR studies on intercalates and organic derivatives of crystalline (α- and γ-forms) zirconium phosphate and zirconium phosphate-phosphite. J. Radioanal. Nucl. Chem. 241 (1), 83–91. https://doi.org/10.1007/BF02347293.

Rajesh, R.U., Dhanaraj, S., 2023. A critical review on quercetin bioflavonoid and its derivatives: Scope, synthesis, and biological applications with future prospects. Arabian J. Chem. 16 (8). https://doi.org/10.1016/j.arabjc.2023.104881.

Tai, N.L., Ghasemlou, M., Adhikari, R., Adhikari, B., 2021. Starch-based isocyanate- and non-isocyanate polyurethane hybrids: A review on synthesis, performance and biodegradation. Carbohydr. Polym. 265. https://doi.org/10.1016/j.carbpol.2021.118029.

Wang, Q., Wang, Z., Ding, K., Wang, L., Gao, C., Zhu, G., 2021. Novel amidoxime-functionalized SBA-15-incorporated polymer membrane-type adsorbent for uranium extraction from wastewater. J. Water. Pro. Eng. 43. https://doi.org/10.1016/j.jwpe.2021.102316.

Wei, Y., Salih, K.A.M., Rabie, K., Elwakeel, K.Z., Zayed, Y.E., Hamza, M.F., Guibal, E., 2021. Development of phosphoryl-functionalized algal-PEI beads for the sorption of Nd(III) and Mo(VI) from aqueous solutions-Application for rare earth recovery from acid leachates. Chem. Eng. J. 412. https://doi.org/10.1016/j.cej.2020.127399.

Yang, L., Huang, C., Luo, X., Zhang, L., Ye, Y., Jun, H., Wang, Y., 2021. Chitosan-based aerogel with anti-swelling for U(VI) adsorption from aqueous solution. Colloids Surf., A. 630. https://doi.org/10.1016/j.colsurfa.2021.127527.

Yuan, G., Li, Y., Yu, Y., Lei, Y., Liu, F., Liu, D., Pu, X., Xiong, W., 2024. Facile construction of a core-shell structured metal-organic frameworks nanofiber membrane for removing Co(II) from simulated radioactive wastewater. Sep. Purif. Technol. 336. https://doi.org/10.1016/j.seppur.2024.126295.

Yusop, M.F.M., Khan, M.N.N., Zakaria, R., Abdullah, A.Z., Ahmad, M.A., 2023. Mass transfer simulation on remazol brilliant blue R dye adsorption by optimized teak wood Based activated carbon. Arabian J. Chem. 16 (6). https://doi.org/10.1016/j.arabjc.2023.104780.

Zeng, D., Dai, Y., Zhang, Z., Wang, Y., Cao, X., Liu, Y., 2020. Magnetic solid-phase extraction of U(VI) in aqueous solution by Fe3O4@hydroxyapatite. J. Radioanal. Nucl. Chem. 324 (3), 1329–1337. https://doi.org/10.1007/s10967-020-07148-y.

Zhang, Z., Li, Z., Dong, Z., Yu, F., Wang, Y., Wang, Y., Cao, X., Liu, Y., Liu, Y., 2022. Synergy of photocatalytic reduction and adsorption for boosting uranium removal with PMo12/UiO-66 heterojunction. Chin. Chem. Lett. 33 (7), 3577–3580. https://doi.org/10.1016/j.cclet.2022.01.062.

Zhang, X.J., Ma, T.Y., Yuan, Z.Y., 2008. Synthesis of hierarchically meso-/macroporous titanium tetraphosphonate materials with large adsorption capacity of heavy metal ions. Chem. Lett. 37 (7), 746–747. https://doi.org/10.1246/cl.2008.746.

Zong, P., Wang, S., Zhao, Y., Wang, H., Pan, H., He, C., 2013. Synthesis and application of magnetic graphene/iron oxides composite for the removal of U(VI) from aqueous solutions. Chem. Eng. J. 220, 45–52. https://doi.org/10.1016/j.cej.2013.01.038.